SUPPORTING INFORMATION

Mechanism of repair of the acrolein- and malondialdehyde-derived exocyclic guanine adducts by the α-ketoglutarate/Fe(II) dioxygenase AlkB

Vipender Singh[†,‡,§,ǁ], Bogdan I. Fedeles[†,‡,§,ǁ], Deyu Li[†,‡,§,ǁ], James C. Delaney[†,‡,§,⊥], Ivan D. Kozekov[Δ], Albena Kozekova[Δ], Lawrence J. Marnett[Δ], Carmelo J. Rizzo[Δ], and John M. Essigmann[†,‡,§,*]

Departments of [†]Biological Engineering, [‡]Chemistry and [§]Center for Environmental Health Sciences, Massachusetts Institute of Technology, Cambridge, Massachusetts 02139, USA

[Δ]Departments of Chemistry and Biochemistry, Center in Molecular Toxicology, Vanderbilt Institute of Chemical Biology and Vanderbilt-Ingram Cancer Center, Vanderbilt University Medical Center, Nashville, TN 37232, USA.

[ǁ]These authors contributed equally.

Present Address

[⊥]Visterra Inc., Cambridge, MA 02139

Corresponding Author

[*]To whom correspondence should be addressed. E-mail: jessig@mit.edu.

Table of contents

Figure S1. The -4 charge envelopes showing isotopic resolution among various peaks generated from AlkB repair reactions of a) α-OH-PdG, b) γ-OH-PdG and c) M_1dG within 16-mer oligonucleotides.

Figure S2. Repair of α-OH-PdG-containing 16-mer oligonucleotide by AlkB, focusing on the appearance of peak at 1238.68.

Figure S3. Repair of α-OH-PdG (X) in single- and double-stranded DNA (ssDNA and dsDNA) by AlkB.

Figure S4. Repair of γ-OH-PdG (X) in single- and double-stranded DNA (ssDNA and dsDNA) by AlkB.

Figure S5. Repair of M_1dG (X) in single- and double-stranded DNA (ssDNA and dsDNA) by AlkB.

Figure S6. Reduction of α-OH-PdG by $NaBH_4$.

Figure S7. Reduction of γ-OH-PdG by $NaBH_4$.

Figure S8. Reduction of M_1dG by $NaBH_4$.

Figure S9. Effect of pH on reduction of α-OH-PdG by $NaBH_4$.

Figure S10. MS/MS fragmentation spectrum of 16mer containing α-OH-PdG (structures **1a & 1b,** unreacted starting material) in the incubation of α-OH-PdG with AlkB. The blue diamond marks the parent ion.

Figure S11. MS/MS fragmentation spectrum of 16mer containing dehydrated form of α-OH-PdG (structure **2**) in the incubation of α-OH-PdG with AlkB. The blue diamond marks the parent ion.

Figure S12. MS/MS fragmentation spectrum of 16mer containing γ-OH-PdG (structures **5a &5b**, unreacted starting material) in the reaction of γ-OH-PdG with AlkB. The blue diamond marks the parent ion.

Figure S13. MS/MS fragmentation spectrum of 16mer containing G (structure **6**, repair product) in the incubation of γ-OH-PdG with AlkB. The blue diamond marks the parent ion.

Figure S14. MS/MS fragmentation spectrum of 16mer containing oxidized γ-OH-PdG (structures **3a & 3b**) in the incubation of γ-HOPG with AlkB. The blue diamond marks the parent ion.

Figure S15. MS/MS fragmentation spectrum of 16mer containing M_1dG (structure **7**, unreacted starting material) in the incubation of M_1dG with AlkB. The blue diamond marks the parent ion.
Figure S16. MS/MS fragmentation spectrum of 16mer containing G (structure **6**) in the incubation of M_1dG with AlkB. The blue diamond marks the parent ion.

Figure S17. MS/MS fragmentation spectrum of 16mer containing oxidized M_1dG (structure **8**, epoxide) in the incubation of M_1dG with AlkB. The blue diamond marks the parent ion.

Figure S18. Predicted collision-induced dissociation (CID) fragmentation pattern of the 16mer oligonucleotide. X denotes the lesion or repair reaction intermediate or product. The *m/z* theoretical values of the CID fragments, calculated using Mongo Oligo Mass Calculator v2.06 (http://library.med.utah.edu/masspec/mongo.htm) are shown in Tables S2-S9.

Table S1. Calculated and observed monoisotopic molecular weight of oligonucleotides containing lesions, intermediates, and their PFBHA derivatives. Structures are depicted in Figure 3 in the main text

Table S2. Predicted and observed *m/z* for MS/MS fragmentation patterns displayed in Figure S10 of α-OH-PdG (structures **1a &1b**) 16mer in the incubation of α-OH-PdG with AlkB. Predicted CID fragments are shown in Figure S10.

Table S3. Predicted and observed *m/z* for MS/MS fragmentation patterns displayed in Figure S11 of dehydrated α-OH-PdG (structure **2**) 16mer in the incubation of α-OH-PdG with AlkB. Predicted CID fragments are shown in Figure S11.

Table S4**.** Predicted and observed *m/z* for MS/MS fragmentation patterns displayed in Figure S12 of γ-OH-PdG (structures **5a & 5b**) 16mer in the incubation of γ-OH-PdG with AlkB. Predicted CID fragments are shown in Figure S12.

Table S5. Predicted and observed *m/z* for MS/MS fragmentation patterns displayed in Figure S13 of G (structure **6**) 16mer in the incubation of γ-OH-PdG with AlkB. Predicted CID fragments are shown in Figure S13.

Table S6. Predicted and observed *m/z* for MS/MS fragmentation patterns displayed in Figure S14 of oxidized γ-OH-PdG (structures **3a & 3b**) 16mer in the incubation of γ-OH-PdG with AlkB. Predicted CID fragments are shown in Figure S14.

Table S7. Predicted and observed *m/z* for MS/MS fragmentation patterns displayed in Figure S15 of M_1dG (structure **7**) 16mer in the incubation of M_1dG with AlkB. Predicted CID fragments are shown in Figure S15.

Table S8. Predicted and observed *m/z* for MS/MS fragmentation patterns displayed in Figure S16 of G (structure **6**) 16mer in the incubation of M_1dG with AlkB. Predicted CID fragments are shown in Figure S16.

Table S9. Predicted and observed *m/z* for MS/MS fragmentation patterns displayed in Figure S17 of M_1dG (structure **8**) 16mer in the incubation of M_1dG with AlkB. Predicted CID fragments are shown in Figure S17.

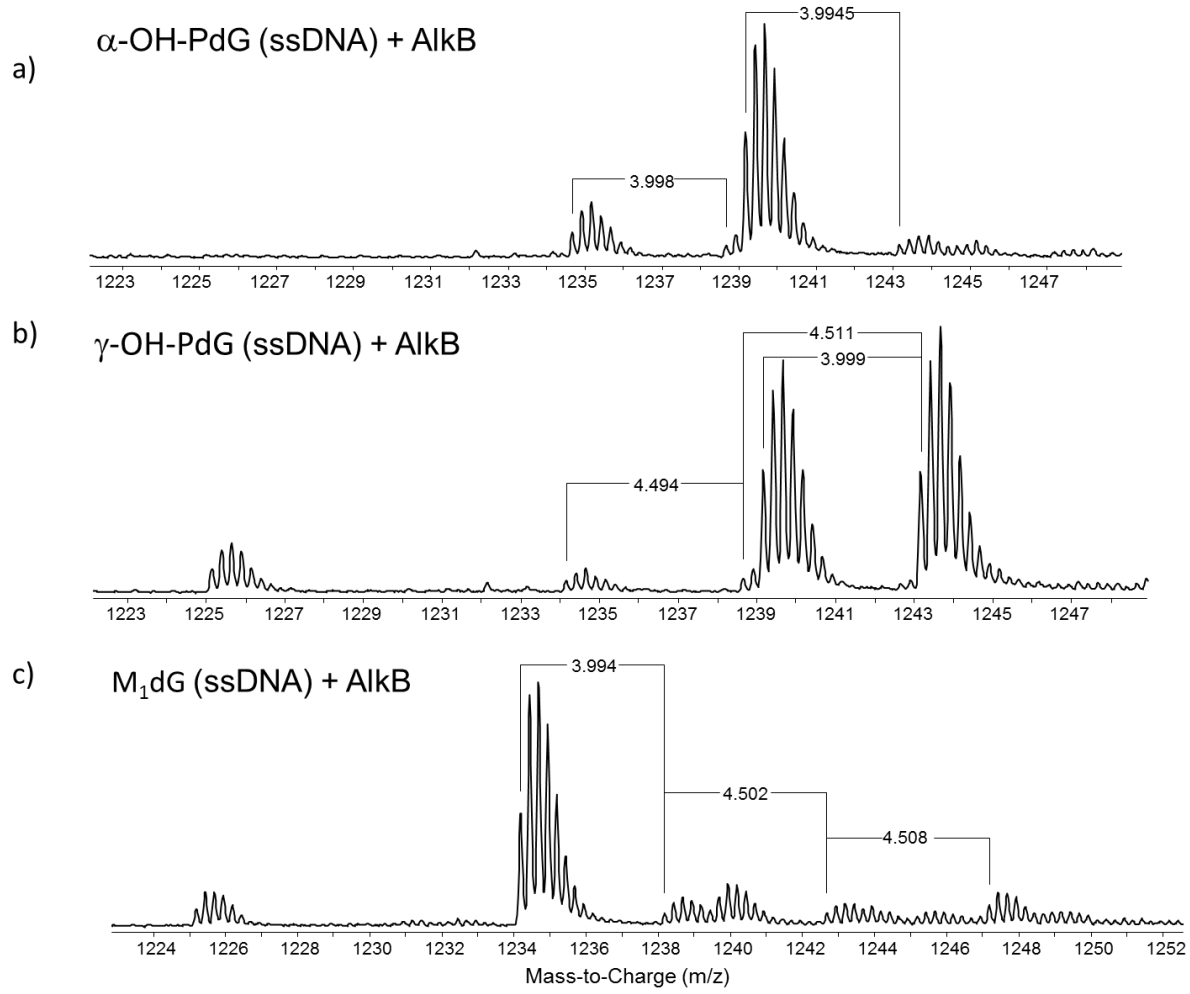

Figure S1. The -4 charge envelopes showing isotopic resolution among various peaks generated from AlkB repair reactions of a) α-OH-PdG, b) γ-OH-PdG and c) M_1dG within 16-mer oligonucleotides.

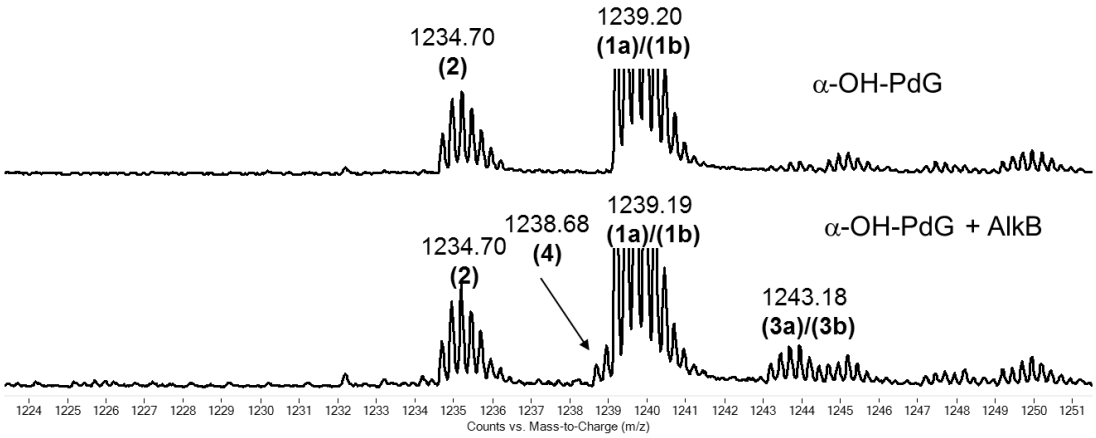

Figure S2. Repair of α-OH-PdG-containing 16-mer oligonucleotide by AlkB, focusing on the appearance of peak at 1238.68.

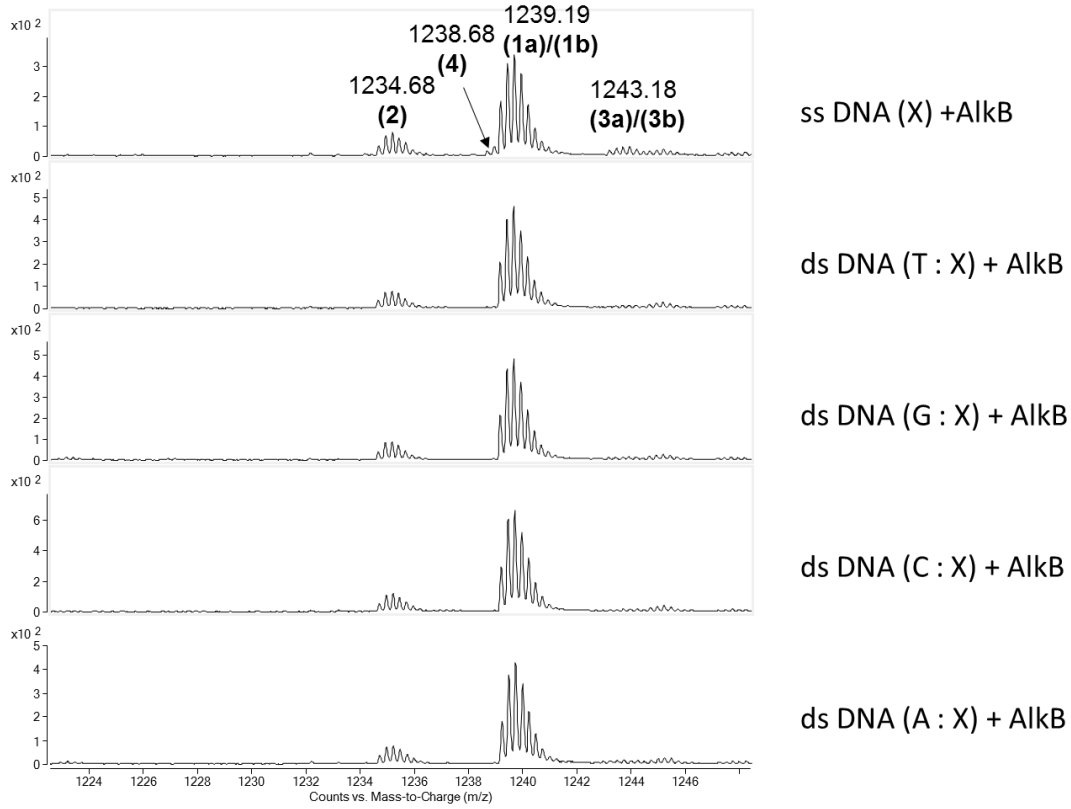

Figure S3. Repair of α-OH-PdG (X) in single- and double-stranded DNA (ssDNA and dsDNA) by AlkB.

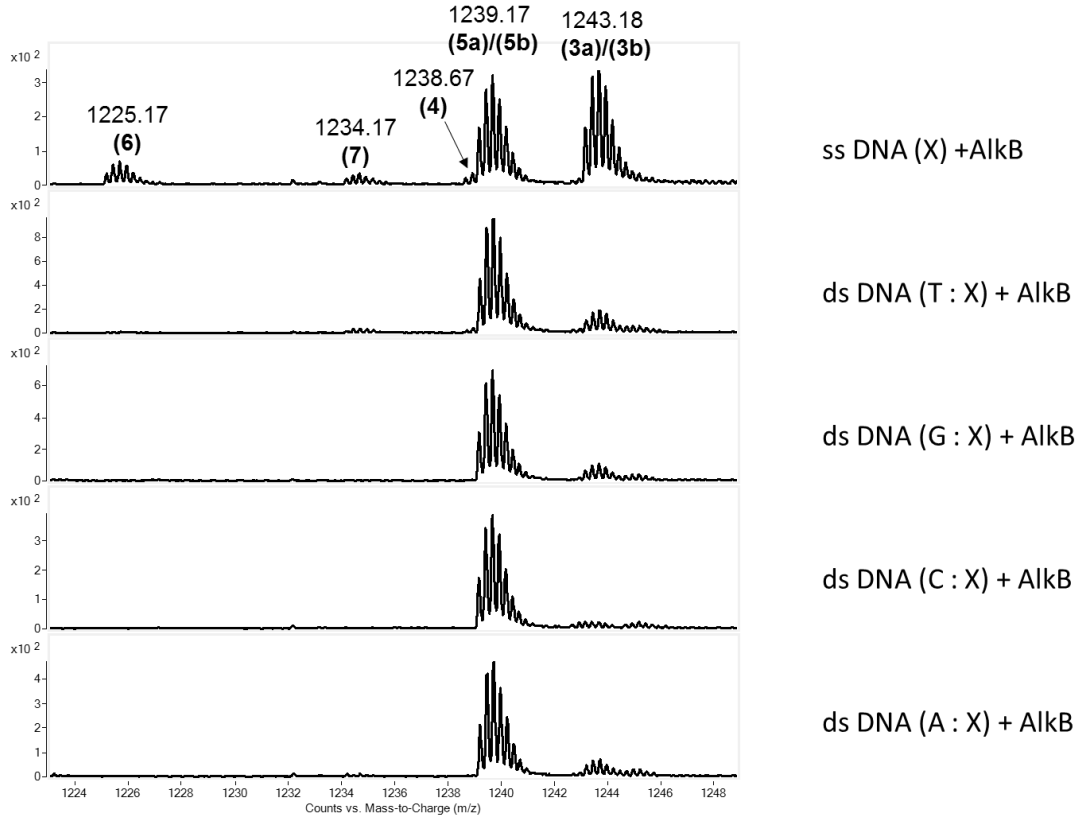

Figure S4. Repair of γ-OH-PdG (X) in single- and double-stranded DNA (ssDNA and dsDNA) by AlkB.

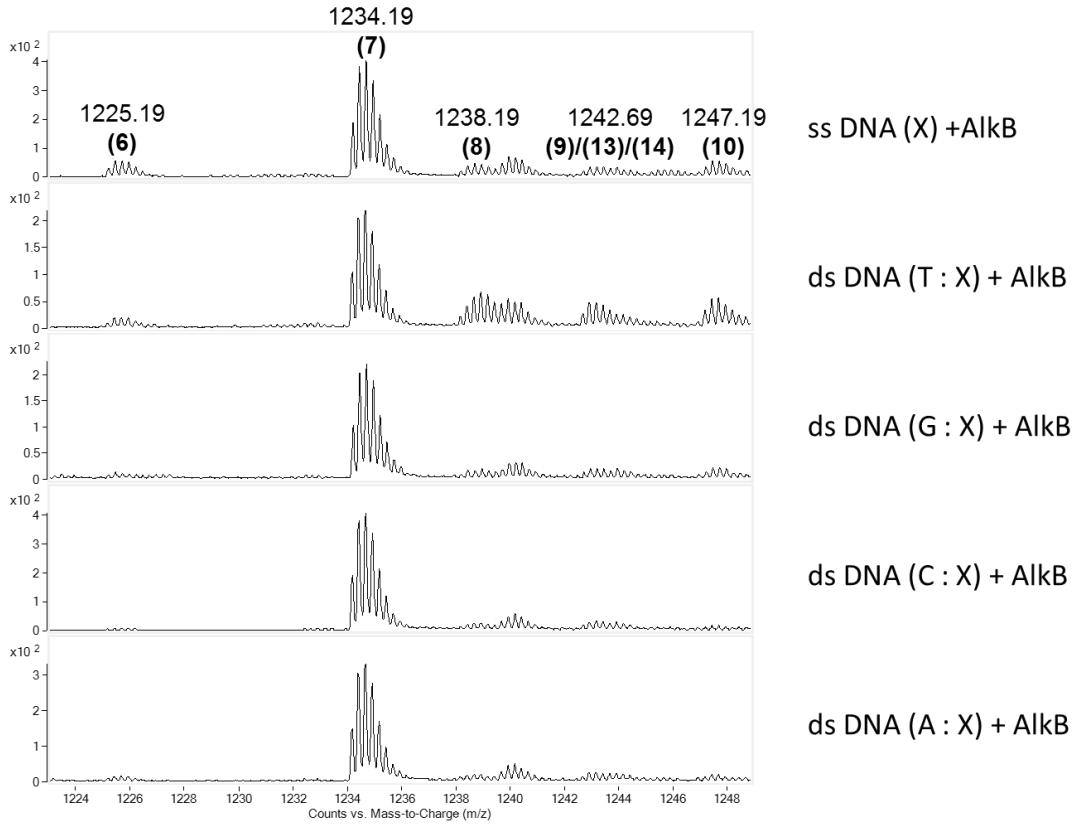

Figure S5. Repair of M_1dG (X) in single- and double-stranded DNA (ssDNA and dsDNA) by AlkB.

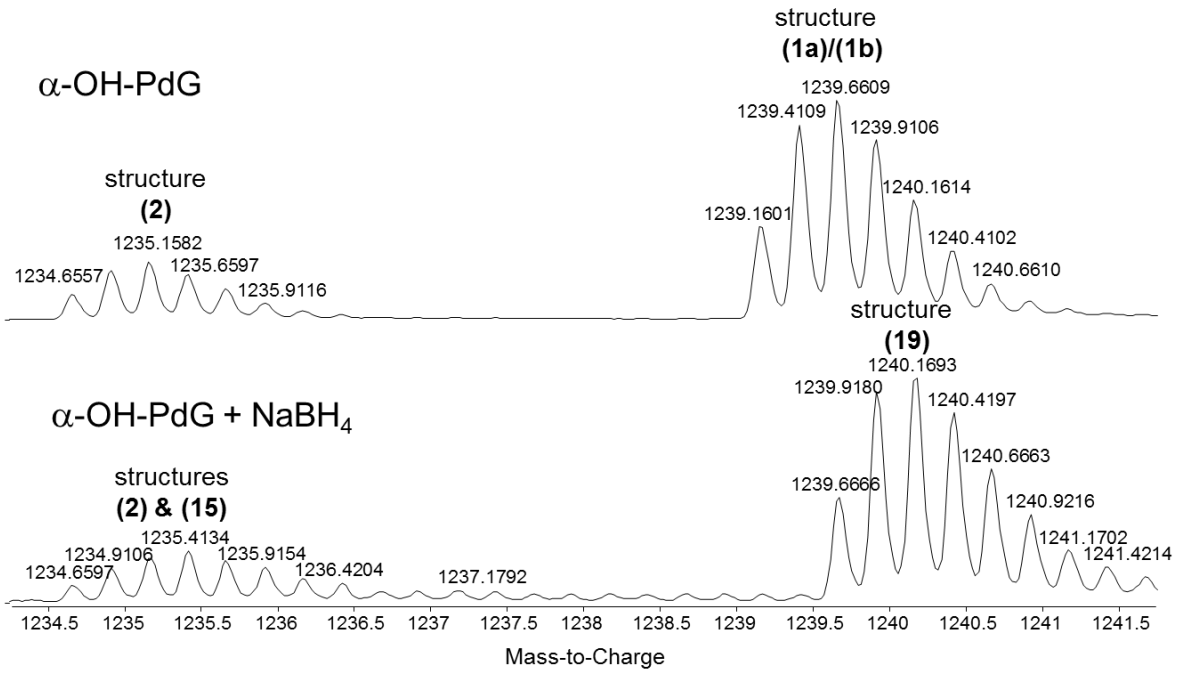

Figure S6. Reduction of α-OH-PdG by $NaBH_4$.

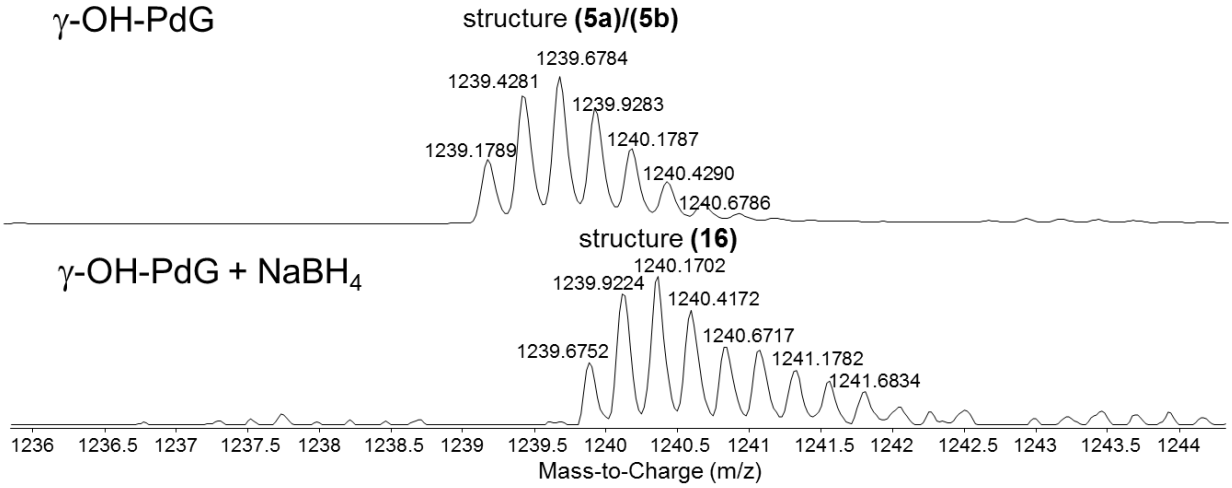

Figure S7. Reduction of γ-OH-PdG by $NaBH_4$.

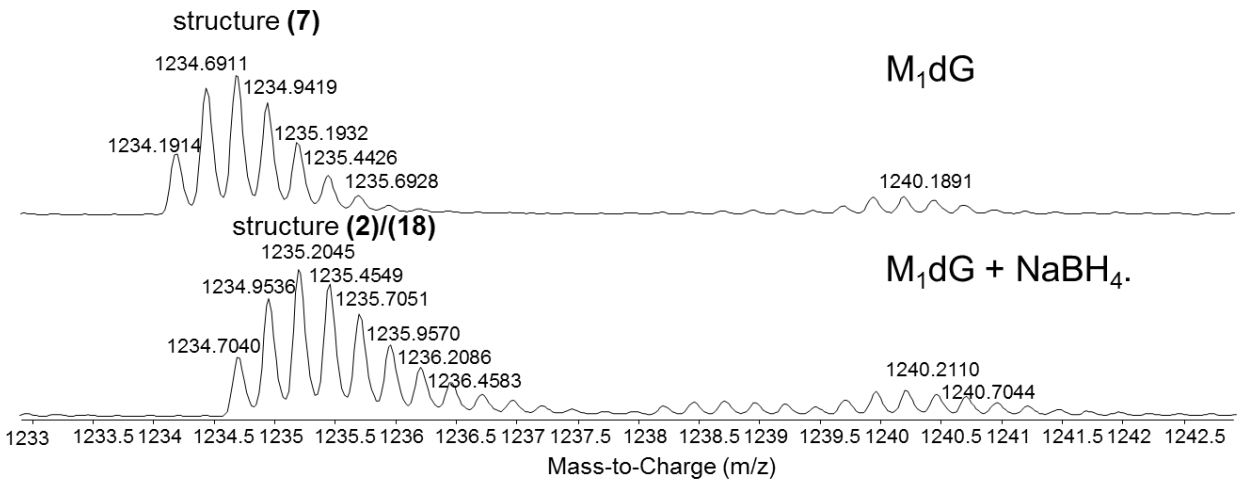

Figure S8. Reduction of M_1dG by $NaBH_4$.

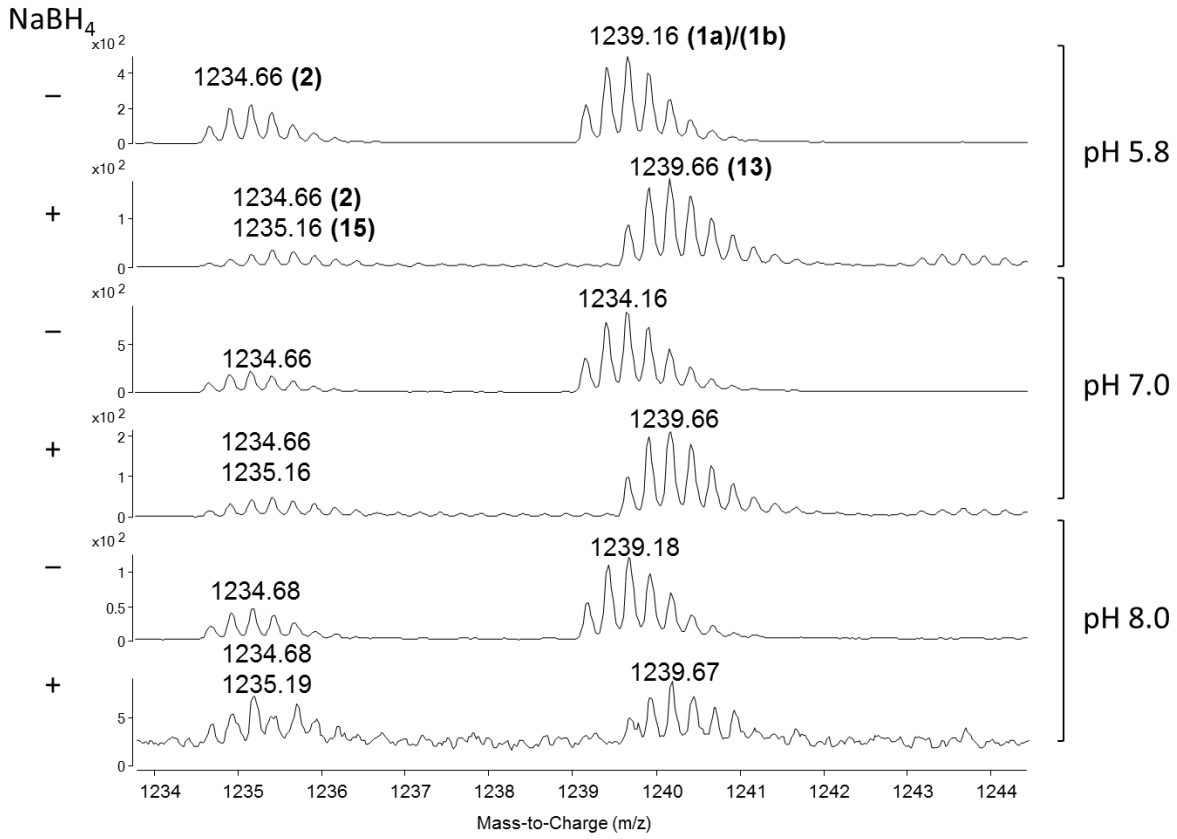

Figure S9. Effect of pH on reduction of α-OH-PdG by $NaBH_4$.

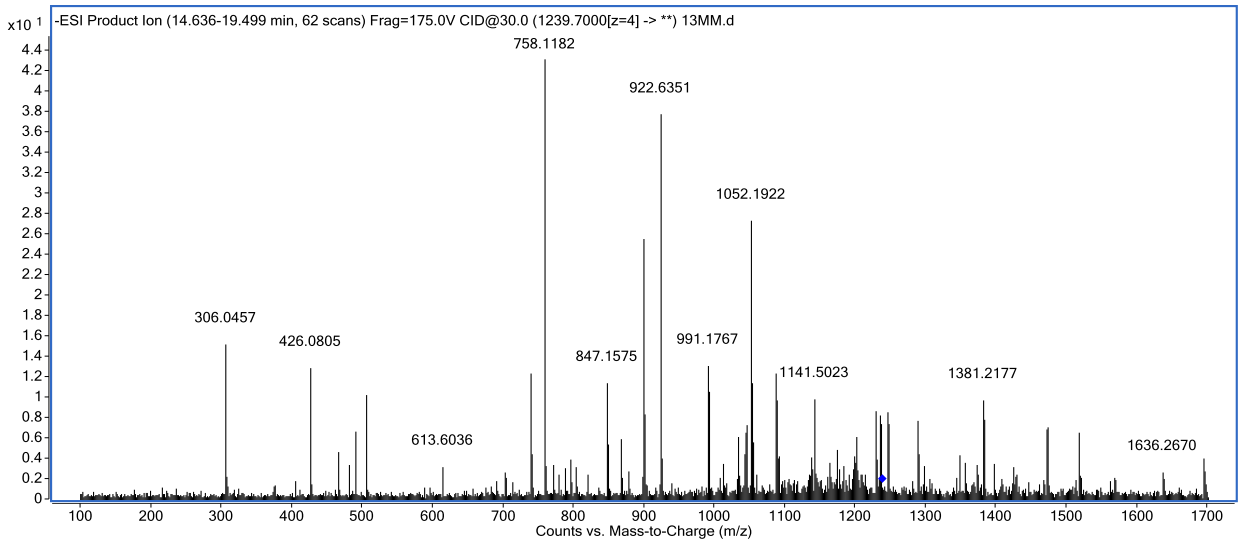

Figure S10. MS/MS fragmentation spectrum of 16mer containing α-OH-PdG (structures **1a & 1b,** unreacted starting material) in the incubation of α-OH-PdG with AlkB. The blue diamond marks the parent ion.

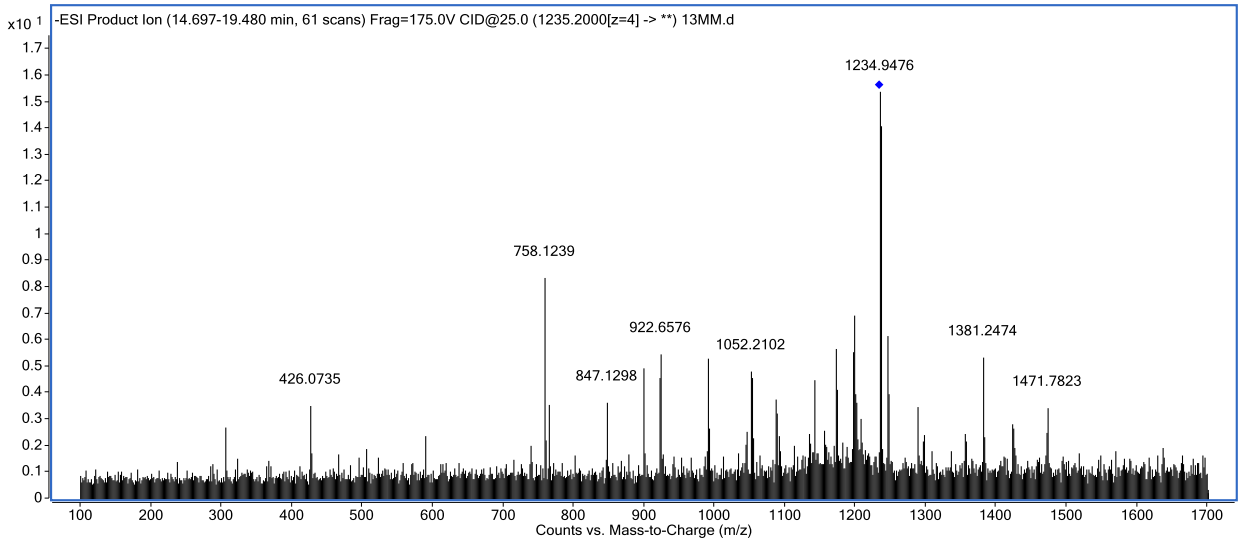

Figure S11. MS/MS fragmentation spectrum of 16mer containing dehydrated form of α-OH-PdG (structure **2**) in the incubation of α-OH-PdG with AlkB. The blue diamond marks the parent ion.

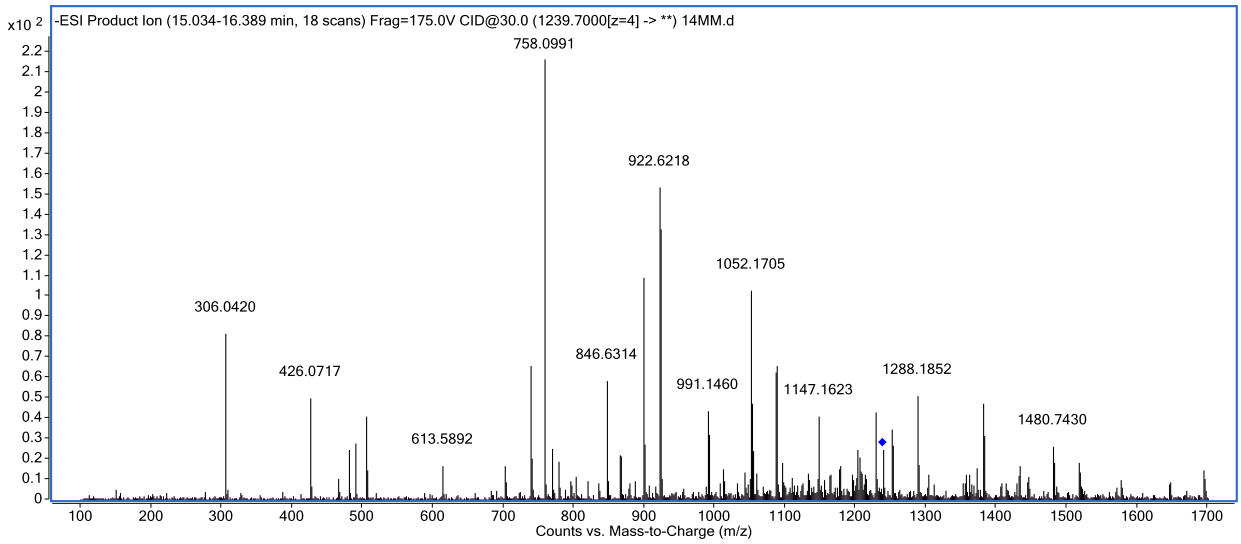

Figure S12. MS/MS fragmentation spectrum of 16mer containing γ-OH-PdG (structures **5a &5b**, unreacted starting material) in the reaction of γ-OH-PdG with AlkB. The blue diamond marks the parent ion.

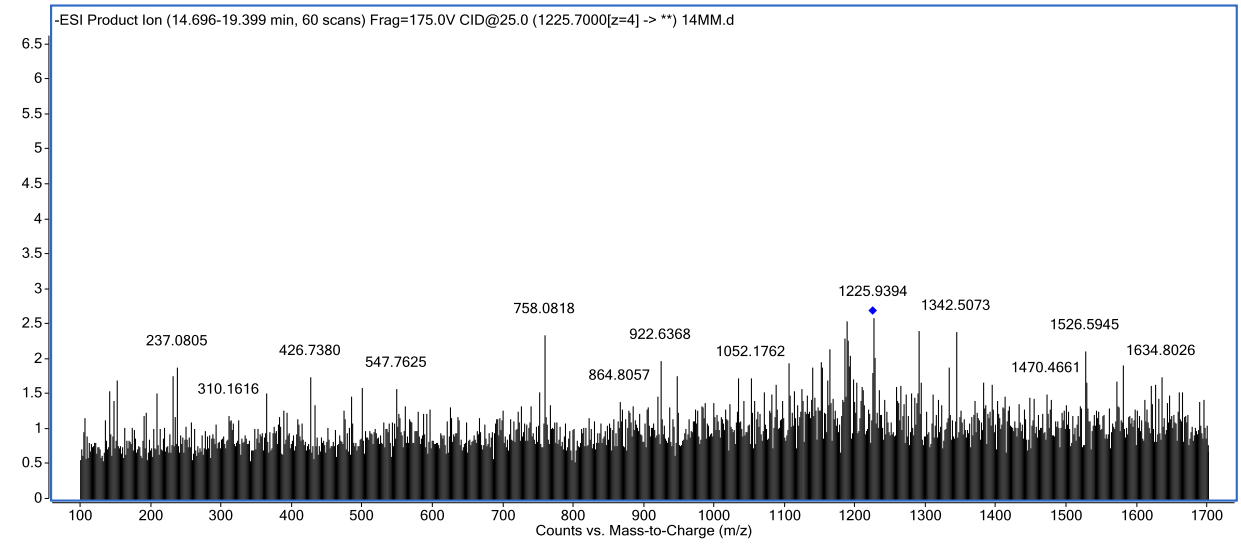

Figure S13. MS/MS fragmentation spectrum of 16mer containing G (structure **6**, repair product) in the incubation of γ-OH-PdG with AlkB. The blue diamond marks the parent ion.

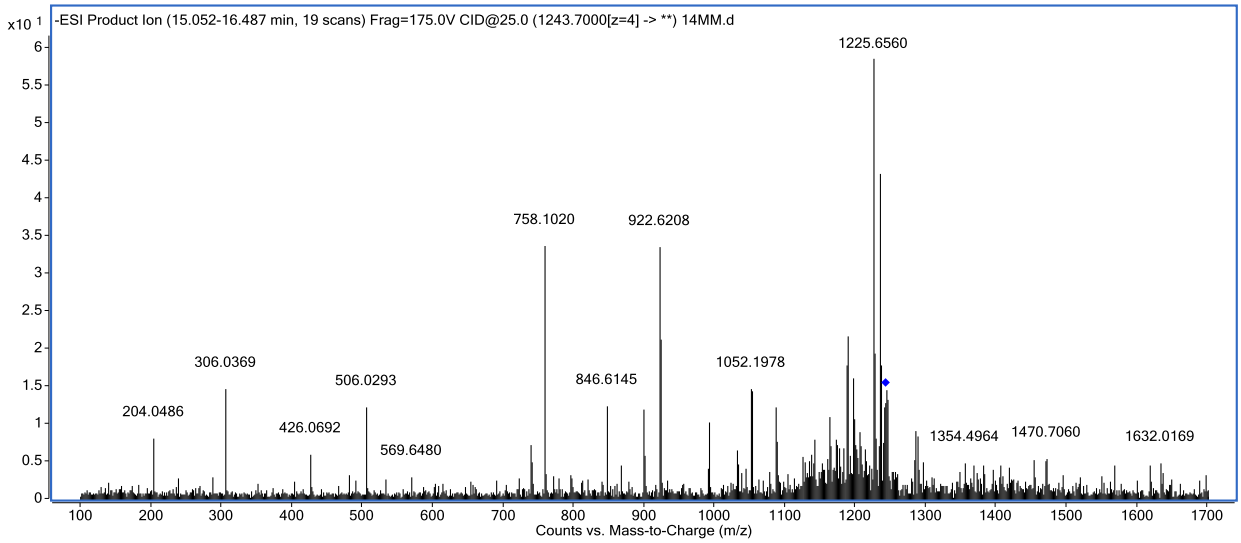

Figure S14. MS/MS fragmentation spectrum of 16mer containing oxidized γ-OH-PdG (structures **3a & 3b**) in the incubation of γ-HOPG with AlkB. The blue diamond marks the parent ion.

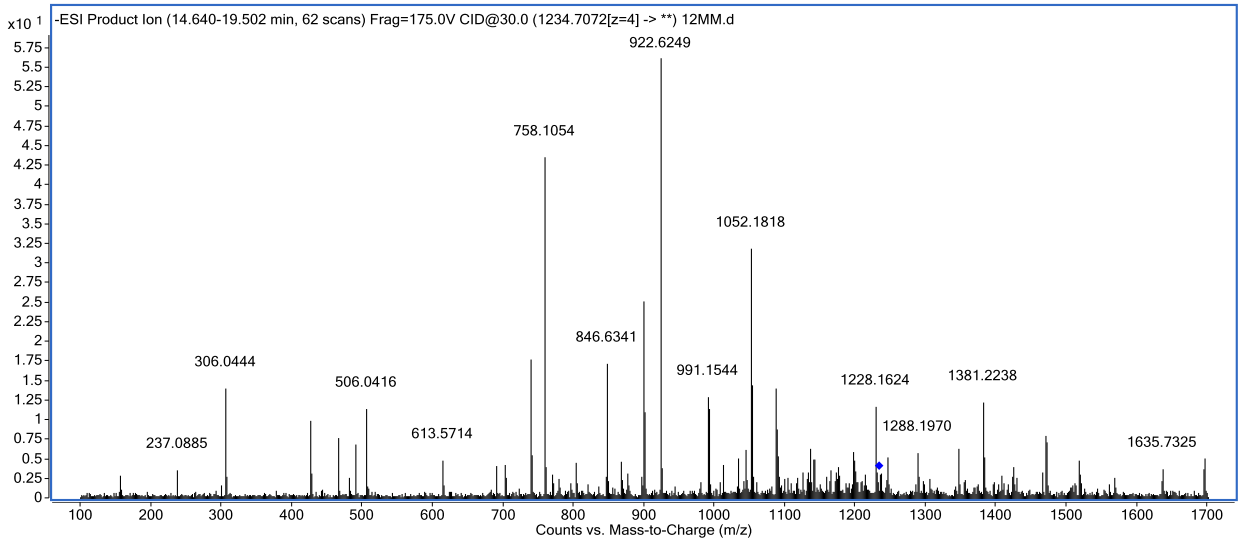

Figure S15. MS/MS fragmentation spectrum of 16mer containing M_1dG (structure **7**, unreacted starting material) in the incubation of M_1dG with AlkB. The blue diamond marks the parent ion.

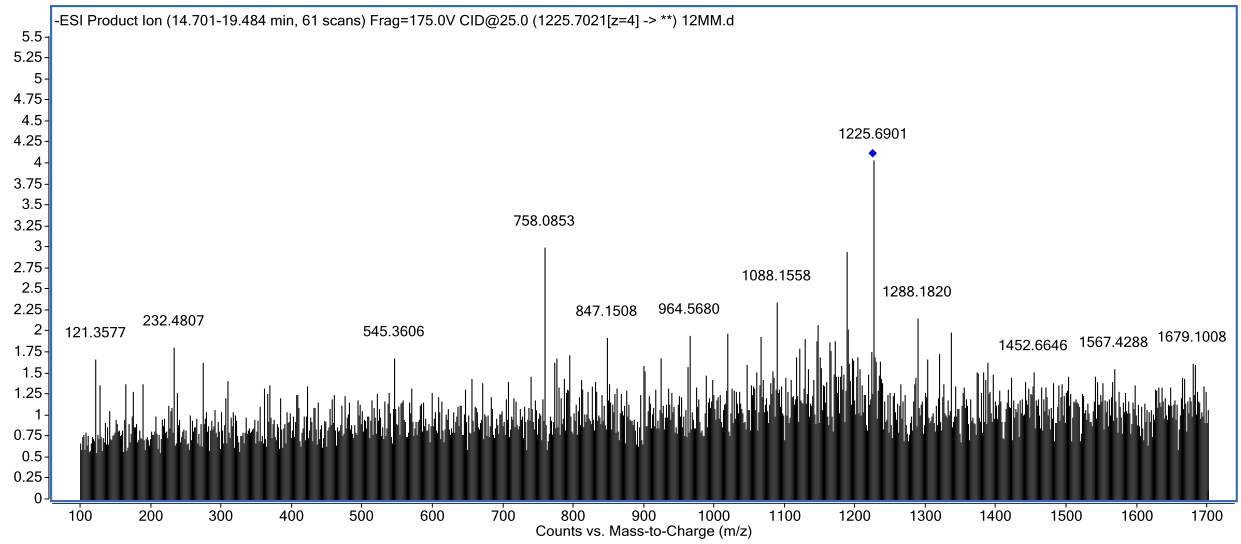

Figure S16. MS/MS fragmentation spectrum of 16mer containing G (structure **6**) in the incubation of M_1dG with AlkB. The blue diamond marks the parent ion.

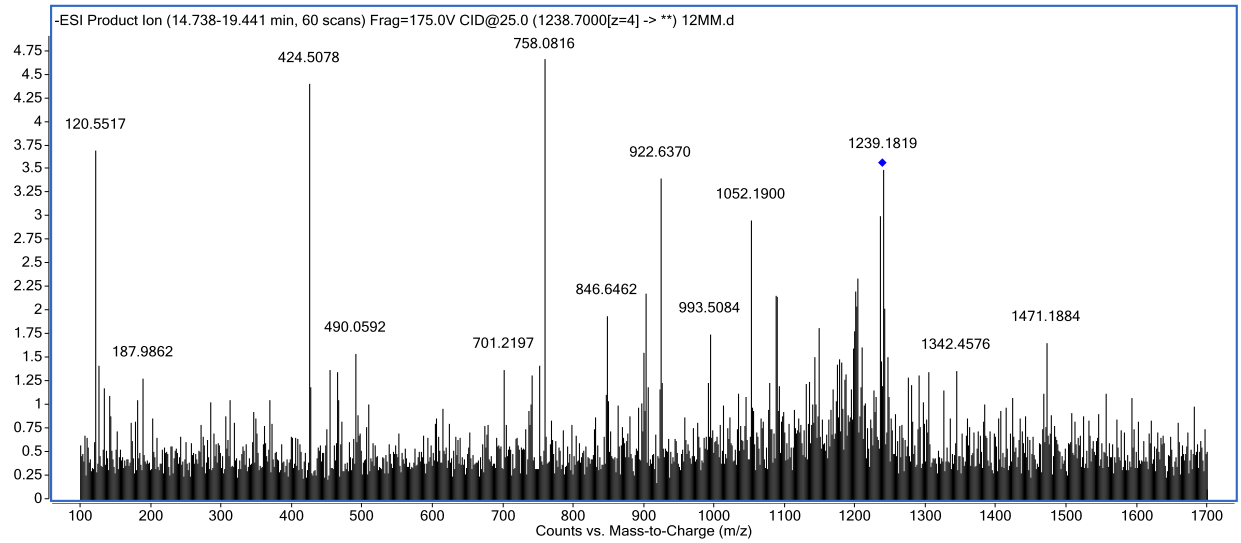

Figure S17. MS/MS fragmentation spectrum of 16mer containing oxidized M1G (structure **8**, epoxide) in the incubation of M_1dG with AlkB. The blue diamond marks the parent ion.

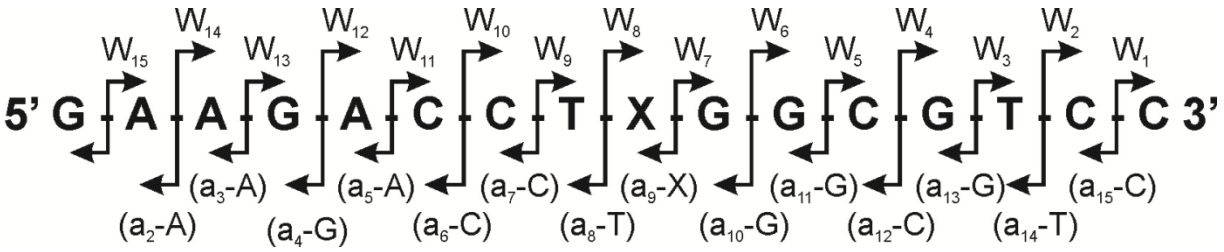

Figure S18. Predicted collision-induced dissociation (CID) fragmentation pattern of the 16mer oligonucleotide. X denotes the lesion or repair reaction intermediate or product. The *m/z* theoretical values of the CID fragments, calculated using Mongo Oligo Mass Calculator v2.06 (http://library.med.utah.edu/masspec/mongo.htm) are shown in Tables S2-S9.

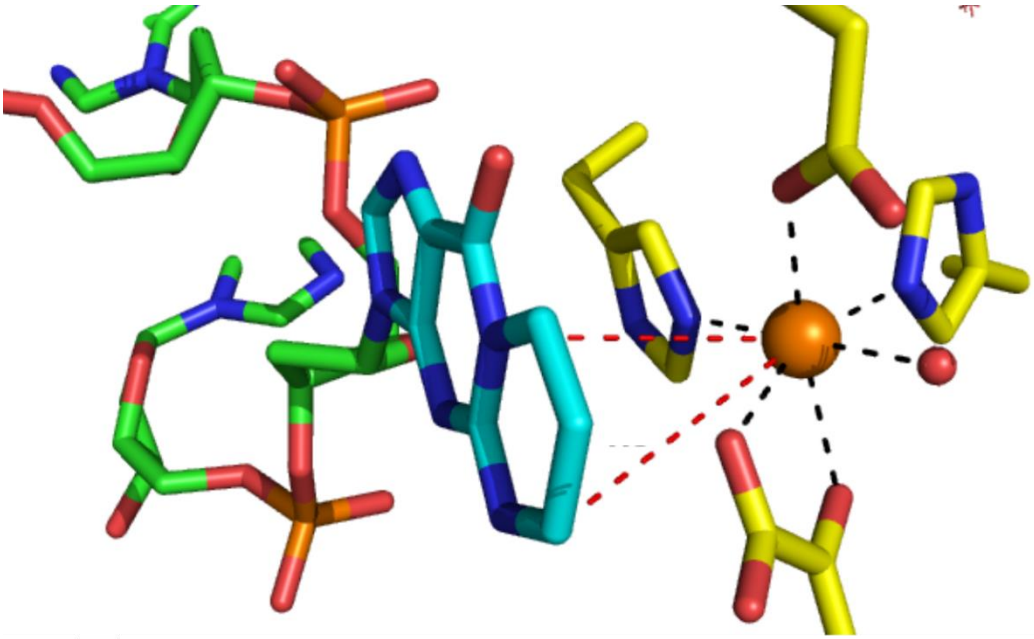

Figure S19. Showing distances between carbons (attached to N1- and N^2- positions) of M_1dG from the Fe in the active site of AlkB. The distances between the carbons attached to the N1 and the N^2- positions are approximately similar (shown in red). These distances are expected to similar for other two exocyclic dG lesions (α-OH-PdG and γ-OH-PdG), because similar to M_1dG both α-OH-PdG and γ-OH-PdG are 3-carbon bridge exocyclic guanine adducts that are attached to the N1 and the N^2-positions of dG.

Table S1. Calculated and observed monoisotopic molecular weight of oligonucleotides containing lesions, intermediates, and their PFBHA derivatives. Structures are depicted in Figure 3 in the main text.

Lesion, base or intermediate	MW (calculated) of neutral species	*m/z* (calculated) -4 charge monoisotopic peak	*m/z* (observed) -4 charge monoisotopic peak
α-OH-PdG **(1b)**	4960.88	1239.21	1239.20/21
α-OH-PdG – H_2O **(2)**	4942.87	1234.71	1234.70/71
(1b) + PFBHA	5155.89	1287.97	1287.98
γ-OH-PdG **(5b)**	4960.88	1239.21	1239.21
(5b) + PFBHA	5155.89	1287.97	1287.97
M_1dG **(7)**	4940.86	1234.21	1234.20
(11b) or (12b) + PFBHA	5153.88	1287.46	1287.47

Table S2. Predicted and observed *m/z* for MS/MS fragmentation patterns displayed in Figure S10 of α-OH-PdG (structures **1a &1b**) 16mer in the incubation of α-OH-PdG with AlkB. Predicted CID fragments are shown in Figure S10.

Fragment	**Charge**	**Theoretical *m/z***	**Observed *m/z***
W1	-1	306.048	306.047
W2	-1	595.094	595.106
W3	-1	899.139	899.139
W4	-2	613.592	613.595
W5	-2	758.115	758.115
W6	-2	922.641	922.634
W7	-2	1087.167	1087.147
W8	-2	1279.707	1279.670
W9	-2	1431.73	1431.704
W10	-3	1050.499	1050.263
W11	-3	1146.848	1146.898
W13	-4	1360.884	1360.536
W14	-4	1098.676	1098.487
W15	-4	1176.94	1176.951
a2-A	-1	426.080	426.077
a3-A	-1	739.137	739.132
a4-G	-1	1052.195	1052.193
a5-A	-1	1381.247	1381.216
a6-C	-2	846.648	846.648
a7-C	-2	991.171	991.173
a8-T	-2	1135.694	1135.431
a9-X	-2	1287.717	1287.701
a10-G	-3	986.502	986.030
a11-G	-3	1096.186	1096.191
a12-C	-3	1205.87	1205.566
a13-G	-3	1302.219	1302.522
a14-T	-3	1411.903	1411.834
a15-C	-3	1513.251	1513.163

Table S3. Predicted and observed *m/z* for MS/MS fragmentation patterns displayed in Figure S11 of dehydrated α-OH-PdG (structure **2**) 16mer in the incubation of α-OH-PdG with AlkB. Predicted CID fragments are shown in Figure S11.

Fragment	**Charge**	**Theoretical *m/z***	**Observed *m/z***
W1	-1	306.048	306.047
W2	-1	595.094	595.092
W3	-1	899.139	899.129
W4	-2	613.592	613.611
W5	-2	758.115	758.120
W6	-2	922.641	922.637
W7	-2	1087.167	1087.178
W8	-2	1270.702	1270.981
W9	-2	1422.725	1422.721
W10	-3	1044.496	1044.473
W11	-3	1140.845	1140.850
W12	-3	1245.197	1245.176
W14	-4	1094.173	1094.363
W15	-4	1172.437	1172.412
a2-A	-1	426.08	426.076
a3-A	-1	739.137	739.147
a4-G	-1	1052.195	1052.195
a5-A	-1	1381.247	1381.275
a6-C	-2	846.648	846.627
a7-C	-2	991.171	991.177
a8-T	-2	1135.694	1135.891
a9-X	-2	1287.717	1287.710
a10-G	-2	1471.252	1471.261
a11-G	-3	1090.183	1090.215
a12-C	-3	1199.867	1199.763
a13-G	-3	1296.215	1296.242
a14-T	-3	1405.899	1405.831
a15-C	-3	1507.248	1507.261

Table S4**.** Predicted and observed *m/z* for MS/MS fragmentation patterns displayed in Figure S12 of γ-OH-PdG (structures **5a & 5b**) 16mer in the incubation of γ-OH-PdG with AlkB. Predicted CID fragments are shown in Figure S12.

Fragment	**Charge**	**Theoretical *m/z***	**Observed *m/z***
W1	-1	306.048	306.042
W2	-1	595.094	595.088
W3	-1	899.139	899.117
W4	-2	613.592	613.582
W5	-2	758.115	758.099
W6	-2	922.641	922.621
W7	-2	1087.167	1087.134
W9	-2	1431.73	1431.690
W10	-3	1050.499	1050.477
W11	-3	1146.848	1146.832
W12	-3	1251.2	1251.181
W15	-4	1176.94	1176.893
a2-A	-1	426.080	426.071
a3-A	-1	739.137	739.123
a4-G	-1	1052.195	1052.171
a5-A	-1	1381.247	1381.217
a6-C	-2	846.648	846.630
a7-C	-2	991.171	991.147
a9-X	-2	1287.717	1287.704
a10-G	-2	1480.257	1480.234
a11-G	-3	1096.186	1096.153
a12-C	-3	1205.87	1205.862
a13-G	-3	1302.219	1302.188

Table S5. Predicted and observed *m/z* for MS/MS fragmentation patterns displayed in Figure S13 of G (structure **6**) 16mer in the incubation of γ-OH-PdG with AlkB. Predicted CID fragments are shown in Figure S13.

Fragment	**Charge**	**Theoretical *m/z***	**Observed *m/z***
W1	-1	306.048	306.056
W2	-1	595.094	595.007
W4	-2	613.592	613.558
W5	-2	758.115	758.084
W6	-2	922.641	922.602
W7	-2	1087.167	1087.135
W11	-3	1128.172	1128.089
W12	-3	1232.524	1232.209
W13	-4	1006.404	1006.368
W15	-4	1162.933	1162.921
a2-A	-1	426.080	426.060
a3-A	-1	739.137	739.098
a5-A	-1	1381.247	1381.172
a6-C	-2	846.648	846.636
a7-C	-2	991.171	991.671
a8-T	-2	1135.694	1135.704
a9-X	-2	1287.717	1287.684
a10-G	-2	1452.243	1452.697
a11-G	-3	1077.510	1077.833
a12-C	-3	1187.194	1187.097
a13-G	-3	1283.543	1283.550

Table S6. Predicted and observed *m/z* for MS/MS fragmentation patterns displayed in Figure S14 of oxidized γ-OH-PdG (structures **3a & 3b**) 16mer in the incubation of γ-OH-PdG with AlkB. Predicted CID fragments are shown in Figure S14.

Fragment	**Charge**	**Theoretical *m/z***	**Observed *m/z***
W1	-1	306.048	306.040
W2	-1	595.094	595.083
W3	-1	899.139	899.112
W4	-2	613.592	613.593
W5	-2	758.115	758.101
W6	-2	922.641	922.622
W7	-2	1087.167	1087.153
W8	-2	1289.702	1289.790
W9	-2	1439.725	1439.617
W10	-3	1055.829	1055.870
W11	-3	1152.178	1152.146
W12	-3	1256.53	1256.588
W13	-4	1024.409	1024.226
W14	-4	1102.673	1102.490
W15	-4	1180.937	1180.950
a2-A	-1	426.080	426.077
a3-A	-1	739.137	739.181
a4-G	-1	1052.195	1052.192
a5-A	-1	1381.247	1381.252
a6-C	-2	846.648	846.617
a7-C	-2	991.171	991.132
a8-T	-2	1135.694	1135.700
a9-X	-2	1287.717	1287.715
a10-G	-2	1488.252	1488.257
a11-G	-3	1101.516	1101.496
a12-C	-3	1211.2	1211.445
a13-G	-3	1307.549	1307.455
a14-T	-3	1417.233	1417.220

Table S7. Predicted and observed *m/z* for MS/MS fragmentation patterns displayed in Figure S15 of M_1dG (structure **7**) 16mer in the incubation of M_1dG with AlkB. Predicted CID fragments are shown in Figure S15.

Fragment	Charge	Theoretical *m/z*	Observed *m/z*
W1	-1	306.048	306.045
W2	-1	595.094	595.130
W3	-1	899.139	899.125
W4	-2	613.592	613.590
W5	-2	758.115	758.107
W6	-2	922.641	922.628
W7	-2	1087.167	1087.152
W8	-2	1269.692	1269.553
W9	-2	1421.715	1421.684
W10	-3	1043.823	1043.799
W11	-3	1140.171	1140.154
W12	-3	1244.524	1244.506
W13	-3	1354.208	1354.141
W14	-3	1458.56	1458.789
W15	-4	1171.932	1171.910
a2-A	-1	426.08	426.077
a3-A	-1	739.137	739.127
a4-G	-1	1052.195	1052.184
a5-A	-1	1381.247	1381.218
a6-C	-2	846.648	846.636
a7-C	-2	991.171	991.152
a8-T	-2	1135.694	1135.562
a9-X	-2	1287.717	1287.688
a10-G	-2	1470.242	1470.205
a11-G	-3	1089.509	1089.461
a12-C	-3	1199.193	1199.149
a13-G	-3	1295.542	1295.531
a15-C	-4	1129.679	1129.769

Table S8. Predicted and observed *m/z* for MS/MS fragmentation patterns displayed in Figure S16 of G (structure **6**) 16mer in the incubation of M_1dG with AlkB. Predicted CID fragments are shown in Figure S16.

Fragment	**Charge**	**Theoretical *m/z***	**Observed *m/z***
W1	-1	306.048	306.052
W3	-1	899.139	899.107
W4	-2	613.592	613.586
W5	-2	758.115	758.085
W6	-2	922.641	922.647
W7	-2	1087.167	1087.219
W9	-2	1403.716	1403.733
W10	-3	1031.823	1031.741
W11	-3	1128.172	1128.129
W12	-4	924.141	924.117
W13	-4	1006.404	1006.532
W14	-3	1446.561	1446.764
W15	-4	1162.933	1162.796
a2-A	-1	426.080	426.057
a3-A	-1	739.137	739.097
a4-G	-1	1052.195	1052.178
a5-A	-1	1381.247	1381.248
a6-C	-2	846.648	846.663
a7-C	-2	991.171	991.137
a8-T	-2	1135.694	1135.773
a9-X	-3	858.142	858.111
a10-G	-3	967.826	967.566
a11-G	-3	1077.510	1077.827
a12-C	-3	1187.194	1187.206
a13-G	-3	1283.543	1283.516
a14-T	-3	1393.227	1393.575
a15-C	-4	1120.679	1120.636

Table S9. Predicted and observed *m/z* for MS/MS fragmentation patterns displayed in Figure S17 of M_1dG (structure **8**) 16mer in the incubation of M_1dG with AlkB. Predicted CID fragments are shown in Figure S17.

Fragment	Charge	Theoretical *m/z*	Observed *m/z*
W1	-1	306.048	306.053
W2	-1	595.094	595.006
W3	-1	899.139	899.135
W4	-2	613.592	613.172
W5	-2	758.115	758.086
W6	-2	922.641	922.628
W7	-2	1087.167	1087.108
W8	-2	1278.255	1278.267
W9	-2	1430.353	1430.448
W10	-3	1049.628	1049.908
W11	-3	1146.023	1146.176
W12	-3	1250.426	1250.271
W14	-3	1464.566	1464.267
W15	-4	1176.475	1176.429
a2-A	-1	426.08	426.073
a3-A	-1	739.137	739.177
a4-G	-1	1052.195	1052.189
a5-A	-1	1381.247	1381.229
a6-C	-2	846.648	846.647
a7-C	-2	991.171	991.188
a8-T	-2	1135.694	1135.623
a9-X	-2	1288.353	1288.219
a10-G	-2	1478.917	1478.893
a11-G	-3	1095.345	1095.316
a12-C	-3	1205.082	1205.045
a13-G	-3	1301.477	1301.447
a14-T	-3	1411.214	1411.226
a15-C	-4	1134.207	1134.162